



This is a repository copy of *An investigation into the role of specimen geometry when undertaking tribological testing on seal fin components.*

White Rose Research Online URL for this paper:

<https://eprints.whiterose.ac.uk/174914/>

Version: Accepted Version

Article:

Zhang, B., Marshall, M. orcid.org/0000-0003-3038-4626 and Lewis, R. (2022) An investigation into the role of specimen geometry when undertaking tribological testing on seal fin components. *Proceedings of the Institution of Mechanical Engineers, Part C: Journal of Mechanical Engineering Science*, 236 (5). pp. 2588-2601. ISSN 0954-4062

<https://doi.org/10.1177/09544062211025058>

Zhang B, Marshall M, Lewis R. An investigation into the role of specimen geometry when undertaking tribological testing on seal fin components. *Proceedings of the Institution of Mechanical Engineers, Part C: Journal of Mechanical Engineering Science*. July 2021. Copyright © 2021 IMechE. DOI: <https://doi.org/10.1177/09544062211025058>. Article available under the terms of the CC-BY-NC-ND licence (<https://creativecommons.org/licenses/by-nc-nd/4.0/>).

Reuse

This article is distributed under the terms of the Creative Commons Attribution-NonCommercial-NoDerivs (CC BY-NC-ND) licence. This licence only allows you to download this work and share it with others as long as you credit the authors, but you can't change the article in any way or use it commercially. More information and the full terms of the licence here: <https://creativecommons.org/licenses/>

Takedown

If you consider content in White Rose Research Online to be in breach of UK law, please notify us by emailing eprints@whiterose.ac.uk including the URL of the record and the reason for the withdrawal request.



eprints@whiterose.ac.uk
<https://eprints.whiterose.ac.uk/>

Title

An Investigation into the Role of Specimen Geometry when Undertaking Tribological Testing on Seal Fin Components

Author

Boxiu Zhang, PhD, Mechanical Engineering, University of Sheffield

Matthew Marshall, Professor, Mechanical Engineering, University of Sheffield

Roger Lewis, Professor, Mechanical Engineering, University of Sheffield

Corresponding author contact information

Dr. Boxiu Zhang

Apartment 21, Smithfield Apartments,

131 Rockingham Street,

Sheffield, UK.

S1 4EY

Other author contact information

Prof. Matthew Marshall

Department of Mechanical Engineering,

Sir Frederick Mappin Building,

Mappin Street,

Sheffield, UK,

S1 3JD

Prof. Roger Lewis

Department of Mechanical Engineering,

Sir Frederick Mappin Building,

Mappin Street,

Sheffield, UK,

S1 3JD

Abstract

Labyrinth seal systems are used in aeroengines to seal the clearance, the understanding of the wear mechanism of labyrinth seal system is necessary to achieve better sealing performance. In this work a series of tests are conducted on a high-speed test rig capable of fin tip speeds of 100m/s. With force and temperature measurements recorded in each case, the influence of specimen geometry is investigated. Surface examination and debris analysis is also performed using microscopy post-test. The wear mechanism was found to be influenced by fin geometry. A discrete fin was observed to trigger a more efficient material removal mechanism at both incursion conditions. Where the fin segment and ring-shaped fin leading to increased temperatures and material smearing. The heat dissipate role of fin was also observed during test where longer contact time of fin and abradable gives better heat removal performance.

Keywords

Wear; Aeroengine; Clearance Control; Coatings; Labyrinth Seal; Abradable; High Speed Test

1 Introduction

To increase the performance of aero-engines, multi-spool shaft designs have been developed and utilised in modern platforms. Whilst a multi-spool shaft increases the overall thermal efficiency of the engine, it also generates new issues. During the operation, especially take off, landing and turning, a multi-spool shaft will deflect. This will lead to the rotating components coming into contact with the surrounding stationary parts of the engine, inevitably leading to abrasion events. Labyrinth seal systems are used in such aero-engines to seal the clearance between turbine blades and the surrounding engine casing, and provide an accommodation for such shaft deflection. An understanding of the material removal mechanism within such a system is therefore necessary to achieve better sealing performance.

In several previous studies [1, 2], testing of abradable materials used in fin seals has typically involved incurring them against a single discrete fin. However, taking the turbine section of an aero-engine as an example, an individual shrouded fin is mounted onto the end of each turbine blade (Figure 1a), with each one joining together to form a single continuous fin around the circumference of the assembly (Figure 1b). During operation, this fin assembly incurs into the abradable lining, and a labyrinth seal is formed. Depending on the severity of this incursion event, contact may take place around the entire circumference of the fin assembly (Figure 1c), with this being typical of running and handling, or over a discrete arc, which frequently occurs during flight manoeuvres when the shaft of the engine moves off-axis. As noted, this situation is significantly different to how these materials are typically tested, where a single discrete fin is mounted within a rotating disc, and a discrete, as opposed to continuous, contact occurs between the fin geometry and the liner test sample.

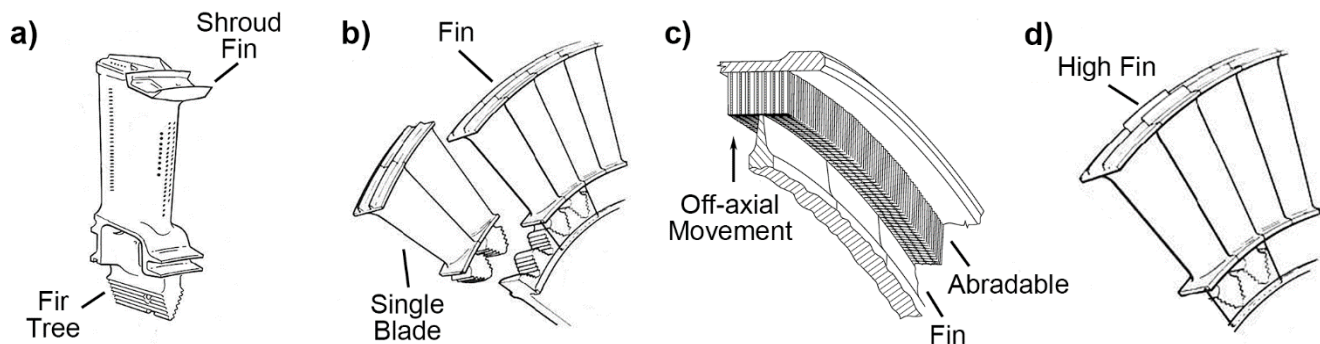


Figure 1 Different contact method under different working condition, a) single blade [3], b) blades assembly [3], c) fin/abradable contacting and d) unmatched fin

Whilst the above describes the design condition for the turbine; it may not always be the case. For example, in situations where the fin assembly is not perfectly round, or a single fin is of greater length than those surrounding it (Figure 1d), a more discretised contact may occur. In this case, the contact conditions may be closer to those of the described test where a single fin is in contact, or indeed over an arc encompassing several fins.

As described in the previous studies [1, 2], during tests with discrete fins the dominant material removal mechanism was via extrusion, along with a limited amount of compacted material either peeling away from the rub track or rebounding behind the contact. Whilst it would appear that the extrusion mechanism is dominant as a consequence of the blunt nature of the fin geometry (Figure 2), given contact is parallel to the flat top surface, it is unclear how much the discrete fin sample has influenced the test, particularly as a

compress and release mechanism is also observed. This latter case is likely only possible as a consequence of the discrete nature of the contact in the test, and may influence the material removal mechanics.

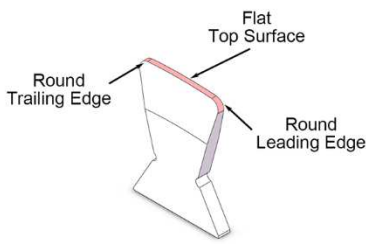


Figure 2 Discrete fin sample geometry

Whilst the topic of labyrinth fin seals is one attracting limited research attention, some studies have attempted to replicate engine conditions more closely. Delebarre et al., investigated the contact between a sealing fin and an Al-Si abrasable material [4-6] using a fully circumferential arrangement consisting of a single circular fin and abrasable sample. Similarly, a continuous circular fin was also employed in Pychynski's [7, 8] and Thévenot's [9] studies where the wear behaviour of a labyrinth-honeycomb seal system was investigated. Recently, Lu investigated the wear behaviour of honeycomb abrasable with segmental fin samples [10] Whilst as discussed these test arrangements go some way to addressing the aforementioned issues surrounding single fin testing, they represent a more complex test, and as such less repeat tests are performed, as well as reduced instrumentation to investigate the contact mechanics. Comparing back to work on compressor blade – liner interactions [11-14], increased insight with respect to wear mechanics has been achieved via a simple, easy to instrument test, where multiple repeats can be performed. Additionally, given the potential range of contact conditions present in the engine, it is in itself important to understand the relationship between contact geometry and wear mechanics.

The aim of this study is to investigate the impact of fin arc length and radius on the material removal mechanism present in a labyrinth fin seal contact, with a specific focus on the forces and temperatures developed. Tests are undertaken using the experimental set up previously detailed for discrete fin samples [1,2], with a new disc employed that is capable of investigating both a long fin segment, as well as a series of segments joined together to form a continuous fin (i.e. a whole ring). By analysing the forces and temperatures developed, along with inspection of the worn samples, changes in the abrasable material removal mechanism as a consequence of the fin arc length are addressed. As such, this study aims to provide a useful insight into how the simplification of considering a single discrete fin for testing impacts on the validity of the results, and how test results can be contextualised with respect to real engine contact conditions.

2 Experimental Methodology & Procedure

2.1 Test samples

Figure 3 shows the three different fin shapes and abrasable samples utilised in this study. A fin segment of 95mm radius is used that can either be placed in isolation or joined together with additional specimens to form a continuous ring. In this study, the segment is used to create two contact scenarios. Firstly, two segments are used 180 degrees opposed with a 90-degree gap between them, in order to create a partial contact, and secondly four segments are used to create a continuous fin geometry in the form of a whole ring. It should also be noted that when the segments are used to create a partial contact, a rounded edge is

introduced to avoid a shock loading as the fin strikes the abradable (Figure 3b). In addition, single discrete fins with 90mm tip radius (Figure 3c) are also employed in order to compare the role of geometry with respect to contact mechanics. Finally, all fin samples are tested against an aluminium silicon based thermally sprayed abradable material (M601NS) with R15Y hardness of 79-82. The abradable is sprayed onto a square steel square backing plate to a thickness of 3mm (Figure 3d), with this being a standard sample size used on the test equipment [2].

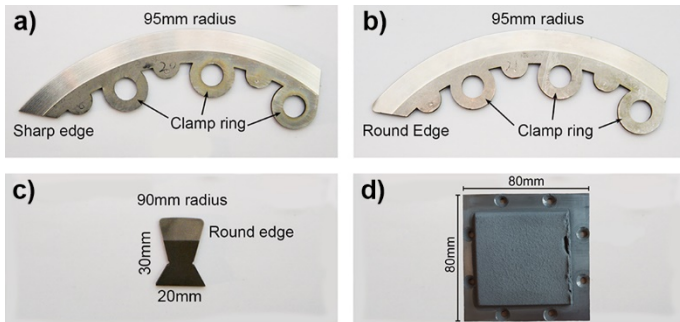


Figure 3 Three different fin samples, a) whole-ring fin, b) fin segment, c) single discrete fin and d) abradable

Aluminium based abrasives, such as M601NS, are typically employed with a titanium alloy-based fin in low-temperature regions of an aero-engine, where a good working performance is achieved. In some cases, this class of abradable is also used in conjunction with more heat resistant fin materials. In this study, a decision was made to manufacture the segments and discrete fins from stainless steel. Comparing back to previous tests with discrete fins [2], investigations of the wear mechanism for fins has suggested that heat is generated through the incursion event, and is not easily dissipated as a consequence of the material removal mechanism combined with the fin geometry. When comparing fins manufactured from titanium to those from a heat resistant superalloy (Inconel 718), high thermal wear was noted with the titanium specimens. As the aim of this study is to specifically investigate the role of geometry on material removal mechanism, a heat resistant fin sample was selected. Whilst Inconel 718 was an option, 304 stainless steel was chosen given its enhanced manufacturability with respect to the sample design, and its similarity in terms of strength and thermal performance to Inconel.

2.2 Test rig and test procedure

Figure 4 shows the test set up utilised in this study. As shown, a rotating disc containing a fin test sample is driven by a spindle with a maximum spindle speed of 21000RPM (GMN HSP-120g, GMN Paul Müller Industrie GmbH & Co. KG, Nürnberg, Germany), and at this rotation rate the fin tip can reach a linear speed of 200ms^{-1} . The abradable sample is mounted onto the top of the microscope stage (OptoSigma SHOT-202, Laser2000 UK Ltd., Northants, UK) and, through movement of the abradable sample towards the rotating fin, an incursion event is achieved. The microscope stage can operate with a speed between 0.1 and $2000\ \mu\text{ms}^{-1}$, meaning a range of different incursion conditions can be created.

The test platform is controlled using a single PC, with a Labview programme setting both incursion conditions as well as recording data from a range of instruments. The sensor system on the test rig consists of a webcam (Logitech C90, Logitech International S.A., Switzerland), a dynamometer (3-Component Force Link Type 9317C, Kistler Instruments Ltd. UK) and a pyrometer (Optris CT XL3 MH1-CF3, Optris GmbH, Germany).

The webcam is used to image the test and determine the level of sparks emitted from the contact, with frames recorded every 50ms using the Labview control programme. Similarly, the dynamometer is installed under the test sample and measures forces over the duration of the test, transferring data to the computer via a signal amplifier. Finally, the pyrometer is focused on the centre of the rub track on the test sample, measuring the temperatures generated. A detailed description of the instrumentation and post-processing is given in the Fois's research article [12].

All tests were conducted following the same procedure; the sample was mounted on the stage, and the fin sample within the disc. With the samples in place, the disc speed, incursion depth, and incursion rate set, and the abradable sample retracted to a distance 500 microns below the rotating fin. Next, the test was commenced with force, temperature and visual results collected by the dynamometer, pyrometer and webcam respectively. In previous studies using this rig [1,2], a stroboscopic imaging system is also utilised, imaging the fin-abradable interaction on a pass by pass basis, thus quantifying wear. It should be noted that in this case, the stroboscopic system was not used, as in the case of the segmental fin samples, wear measurement is not possible given the continuous nature of the sample. Additionally, as shown in Figure 4, an electrically conductive double-sided sticker is set on the side of the abradable to collect the generated debris. During the test, the debris generated by the incursion is ejected by the fin and attaches to the sticker. Following the tests, along with the worn samples, the debris collected via the conductive sticker for each test was analysed using SEM analysis, classifying the size and shape of the debris generated.

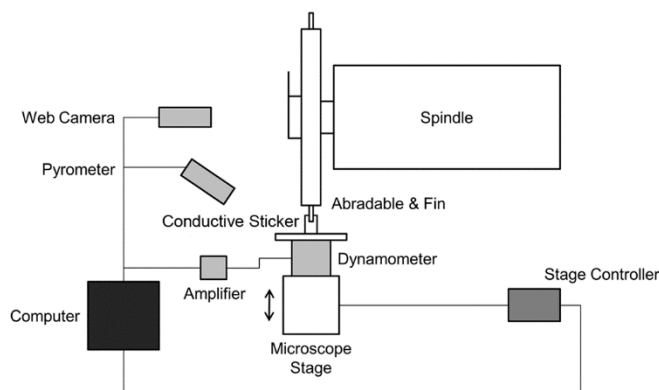


Figure 4 Schematic diagrams of equipment used for the incursion tests

In order to mount the different fin samples, two different discs are used in this study. The segmental fins are installed on the test rig by using the disc shown in Figure 5b. The overall radius of the fin is 90mm when mounted in the disc, and the tip speed range is 0 – 200m/s. As Figure 5b illustrates, there are four fin slots in the middle of the disc, and each slot has three evenly arranged pins on the disc side to fix the position of the segmental fins. Depending on the test performed, two (Figure 5b) or four fin segments (Figure 5c) can be installed in the disc, resulting in a partial or circumferentially continuous fin ring. Finally, twelve grub screws are used to lock the fin segments in the axial direction.

As shown in Figure 5a, a separate disc is used to undertake tests with a discrete fin sample. In this case, a single test fin is mounted within a slot on the disc, with a dummy fin mounted diametrically opposed for balancing. In order to prevent the dummy fin interacting with the sample surface, it is positioned 2mm closer to the centre of the disc, with appropriate geometric differences made to its form to ensure a dynamic balance

is achieved. As shown in the Figure 5a, the fin samples are held in place via sliding block and locking pin arrangement, thus preventing movement during a test.

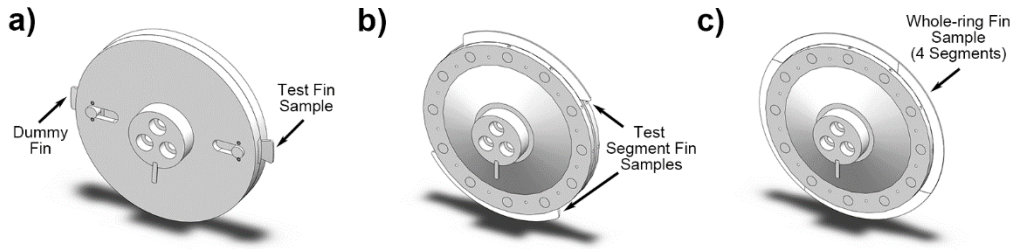


Figure 5 a) discrete fin disc, b) Segment fin disc and c) whole-ring fin disc used in this study

2.3 Test matrix

Table 1 details the incursion conditions for the tests performed. As detailed in Section 2.1, three 10mm diameter pins are used to mount the fin segments in place. On initial testing of the new disc design, it was found that the centrifugal forces developed led to localised yield of the fin segments in some cases. It was determined that the upper tip speed limit in order to prevent this occurring was 140m/s. Comparing back to previous testing of fin seal – abrasible interactions [2], it was determined that engine representative wear mechanics occurred at a tip speed of 100m/s. Indeed, this has been a feature of multiple studies on abrasible linings [11-15] and as such tests were performed at 100m/s.

Previous studies show that for a discrete fin, distinct material removal mechanisms occurred at both 0.02µm/pass (low incursion rate) and 2µm/pass (high incursion rate). At the lower incursion rate, material was compacted and at times ruptured, whereas at the higher rate better dislocation occurred. Therefore, these two incursion rates were once again selected for this study and converted into equivalent incursion speeds for the test with a fin segment, and a complete circumferential fin (whole ring). The equivalent incursion speeds were 3.1µm/s and 310µm/s for the lower and upper conditions respectively.

Table 1 Test matrix for whole-ring, segmental and single discrete fin test

Test Code	Fin Shape	Fin Material	Abradable	Tip Speed [m/s]	Incursion Speed [µm/s]	Incursion Depth [µm]
Test-W-0.02	Whole-ring	St.St.304	M601NS	100	3.1	2000
Test-S-0.02	Segmental	St.St.304	M601NS	100	3.1	2000
Test-N-0.02	Single	St.St.304	M601NS	100	3.1	2000
Test-W-2	Whole-ring	St.St.304	M601NS	100	310	2000
Test-S-2	Segmental	St.St.304	M601NS	100	310	2000
Test-N-2	Single	St.St.304	M601NS	100	310	2000

3 Results

3.1 Abradable and fin samples post-test

Figure 6 shows the abradable and fin samples post-test. Indicated on the abradable sample images are the expected length of the rub tracks, providing an initial visual assessment of whether pick up or wear occurred. It should also be noted that for the fin segments, the trailing edge is shown in each case, as it is at this point that thermal damage was apparent in some cases. Where thermal damage did occur to either the abradable or fin sample, this is evident from changes in colour of the sample surface, where this appears as light grey on the abradable and blue / orange on the blade surface. As shown by Figures 6a, 6c, & 6e, regardless of

type, all fin samples showed evidence of thermal damage at the low incursion speed. However, this was not the case for the corresponding abrasable samples. In the case of the discrete fin (Figure 6e), no thermal damage is present on the abrasable, with a small amount of thermal damage then occurring on the partial segment test (Figure 6c), and increasing for the fully circumferential fin (Figure 6a). At the higher incursion speed, there is no evidence of thermal damage in any of the tests regardless of fin type. Moving onto wear, the discrete fins show increased visual damage at both incursion rates, when compared to the other types of fins investigated. It also noted that the test with the partial fin segment at the higher incursion rate (Figure 6d) was unusual as adhesion rather than wear took place.

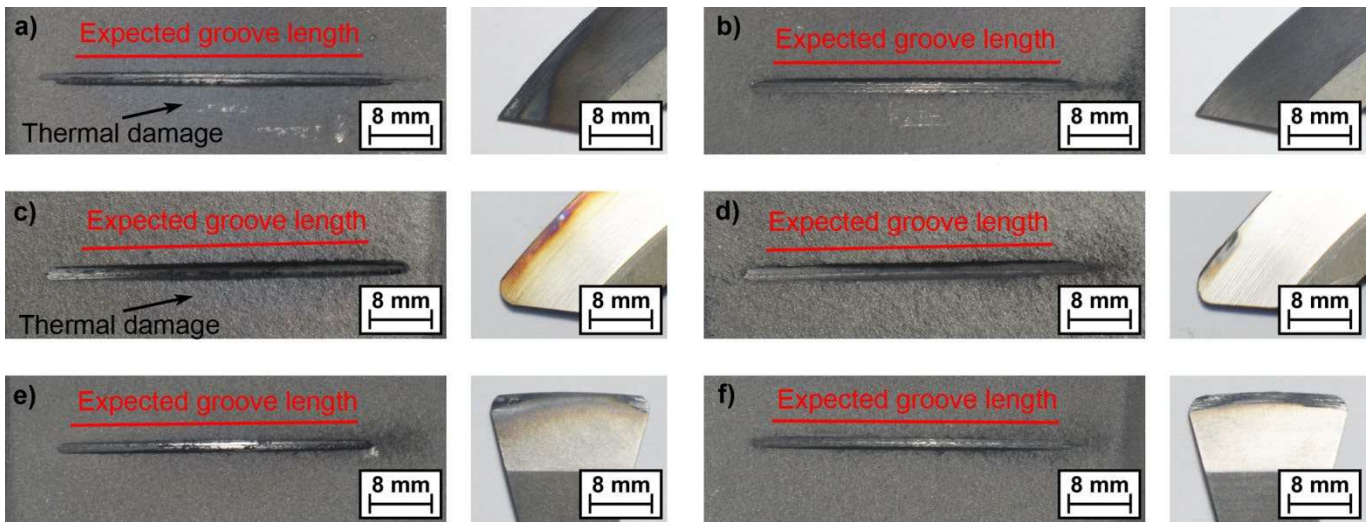


Figure 6 Worn groove and fin profile after testing for test with three types of St.St.304 fin, a) whole ring, 0.02µm/pass, b) whole ring, 2µm/pass, c) segmental, 0.02µm/pass, d) segmental, 2µm/pass, e) single discrete, 0.02µm/pass and f) single discrete, 2µm/pass

In order to better characterise whether adhesion or wear took place during the tests, the expected length of the worn groove on the abrasable was compared to the actual value achieved (Figure 7). The expected groove length was calculated using the 90mm rotating tip radius and 2mm incursion depth. As shown in Figure 6, all worn groove lengths are longer than the expected groove length, indicating that material has adhered to the fin resulting in overcutting. From the measurement of the wear scars, this effect also appears more pronounced at the lower incursion speed, as well as with increasing fin coverage. The exception is for the discrete fin at the low incursion rate, where the least amount of overcutting is observed. Looking back at the fin samples post-test (Figure 6), as indicated on the figure, where adhesion is present it appears to be so at the trailing edge. However, it is also apparent that adhered material is not visible in all cases, indicating that break off may also occur.

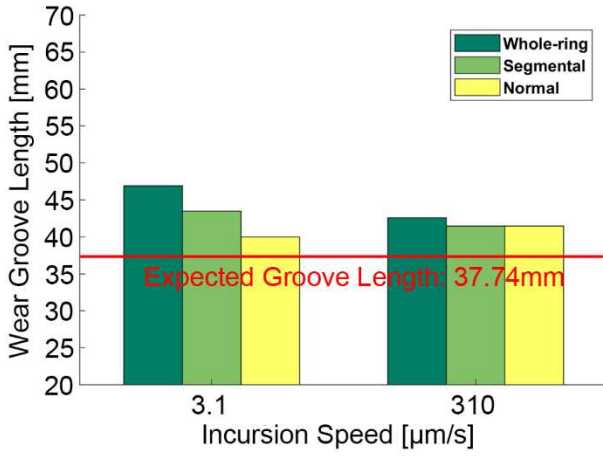


Figure 7 Wear groove length for tests with stainless steel fins

3.2 Force and temperature

The forces and temperatures measured for the whole ring, segment and discrete fin tests are detailed in the following section. It should be noted in the figures that the scale of the x-axis varies as a consequence of both the different fin profiles, as well as for the two incursion speeds tested. With respect to fin sample this is due to varying amounts of circumferential fin coverage, from the discrete fin through to the whole ring, meaning the amount of contact actually occurring in a single revolution is different. For incursion speed, this variation in contact length is simply due to the differing amounts of material being removed per revolution. In the case of a discrete fin, the contact only occurs when the fin passes the abradable sample, and the rub length is counted individually in each pass. Since the rub length per pass grows along with the increase of incursion depth during the test, the total rub length does not linearly relate to test time. In this instance, the total rub length is calculated for the test using the following equation:

$$L = \sum_{i=1}^n \cos^{-1} \left(\frac{r - ir \times i \div (1 \times 10^6)}{r} \right) \times r \quad \text{Equation 1}$$

where r is fin rotation radius and ir is incursion rate.

The equation stated above is applied when the contact condition is assumed close to that of a point contact, as is the case for the single discrete fin sample. Where the segmental fins are used, and the fin is in contact for either 50% or the total duration of the test time, the relationship between time domain and rub length domain can be simplified into the following equation:

$$L = CR \times v \times t \quad \text{Equation 2}$$

where v is tip speed, t is test time, and CR represents the fraction of the circumference shrouded by the fin.

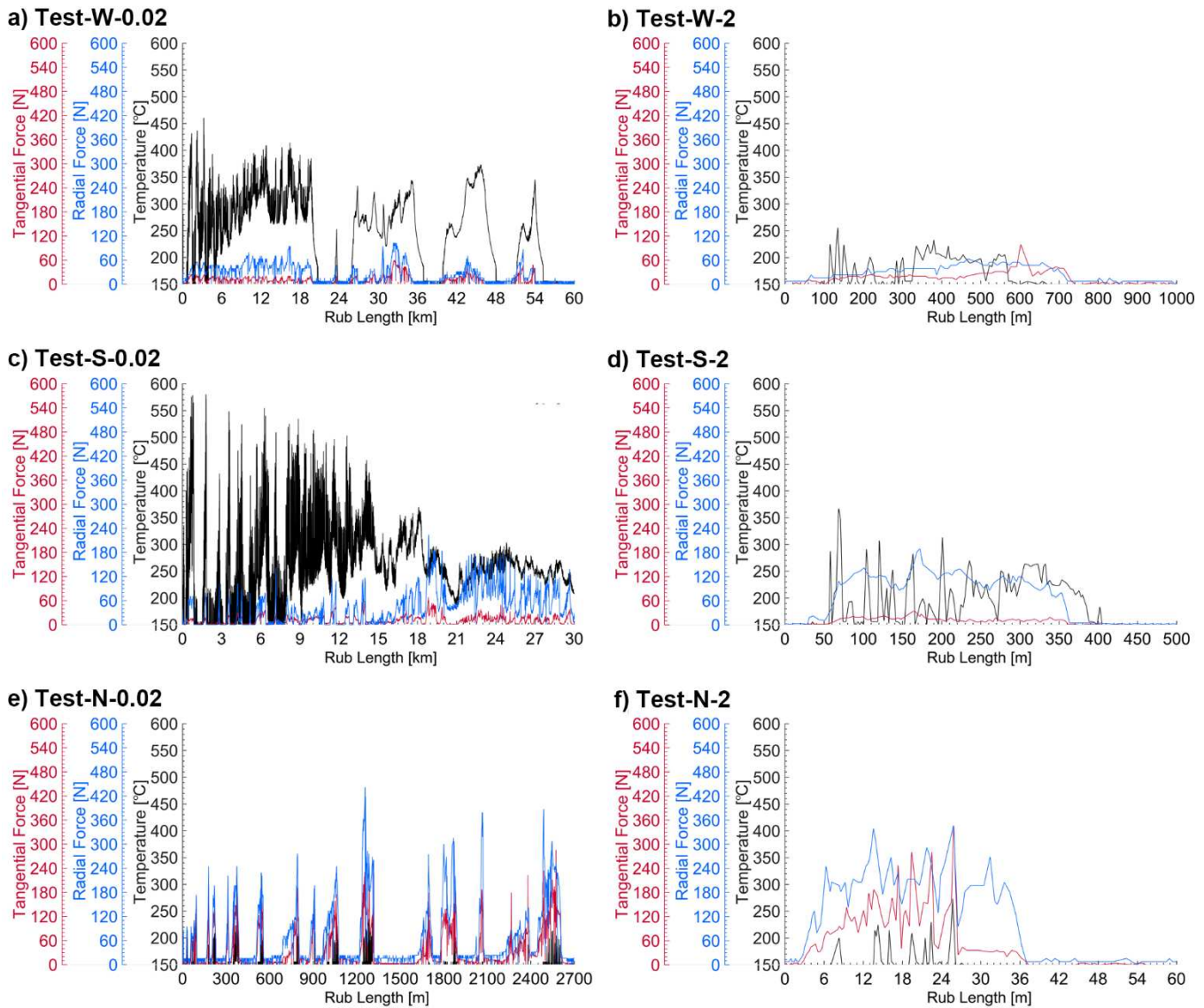


Figure 8 Force and temperature results of tests with three types of St.St.304 fin, a) whole ring, 0.02 μ m/pass, b) whole ring, 2 μ m/pass, c) segmental, 0.02 μ m/pass, d) segmental, 2 μ m/pass, e) single discrete, 0.02 μ m/pass and f) single discrete, 2 μ m/pass

Figure 8 shows the forces and temperature results for the different tests performed. In the case of the low incursion speed with the single fin (Figure 8e), cyclic behaviour is clearly evident, with forces and temperatures periodically rising before falling away. Comparing all the tests undertaken at the low incursion condition for the different fin types (Figures 8a, 8c, and 8e), it is clear that the total rub length of the tests with the whole ring and fin segments is much longer than that of the discrete fin test, due to the long arc length of the fin tip in these cases. This makes it difficult to assess whether cyclic behaviour similarly occurs for these tests at low incursion rate. In order to investigate this point further, the force and temperature data from the first 2700m of the tests was replotted (Figure 9). As shown in the figure, cyclic behaviour is also evident in the tests with the whole ring and segmented fins, where it can be seen that for the tests with longer contact lengths, forces are lower and temperatures higher, when compared to those of the discrete fin. The frequency of the cyclic behaviour is also reduced in these two cases. Finally, it is also interesting to note that the highest temperatures occur in the case of the segmented test. Going back to Figure 8a and 8c for the whole ring and segmented fin respectively, it is also apparent that the cyclic behaviour does not continue in exactly the same manner throughout the tests. In both cases overtime peaks become less discrete with periods of more continuing forcing or high temperature, again marking a difference when compared to the discrete fin result.

In the case of the higher incursion rate tests (Figures 8b, 8d, and 8f), cyclic behaviour was not observed for any of the fin types investigated. Broadly the force and temperature results were of similar form, with continual variation around a mean value, and varying magnitudes based on fin type. Once again, forces were highest in the case of the discrete fin (Figure 8f), and lowest for the whole ring (Figure 8b). Similarly, the highest temperatures were also once again present in the case of the segmented fin (Figure 8d).

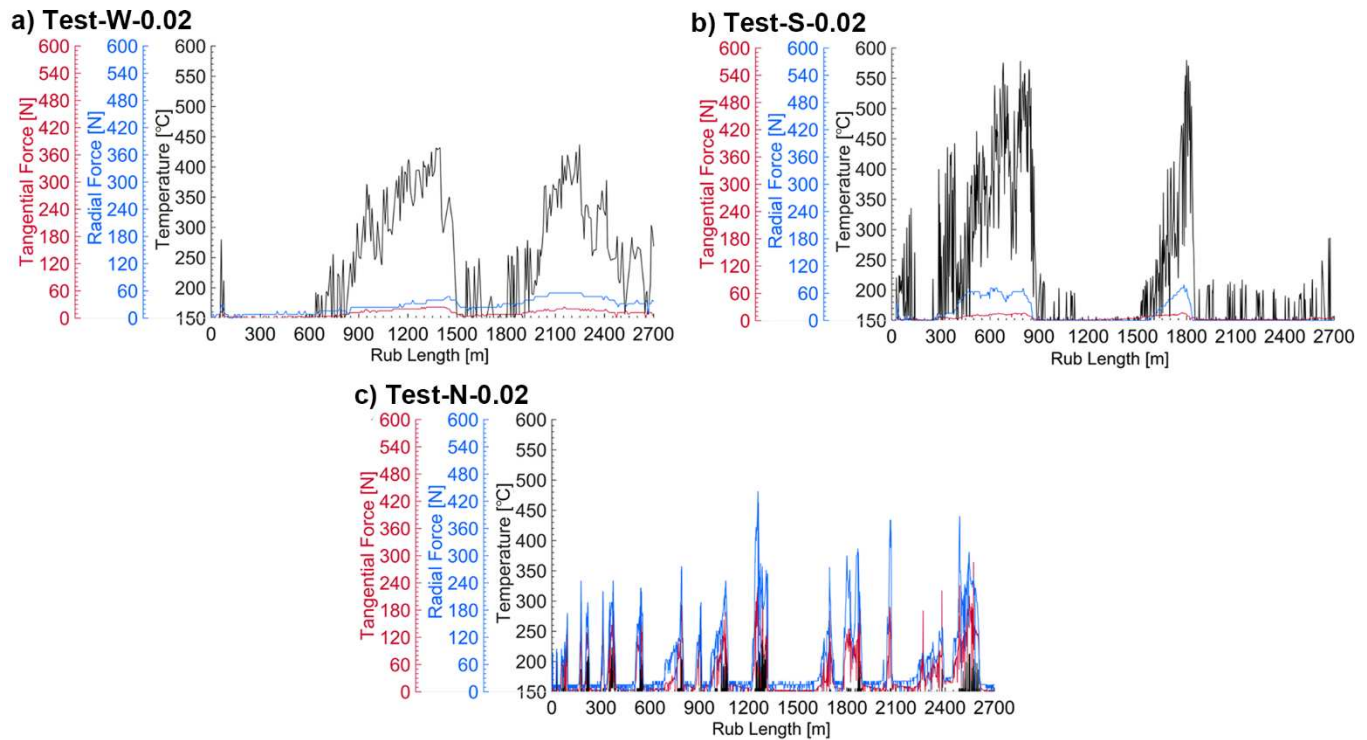
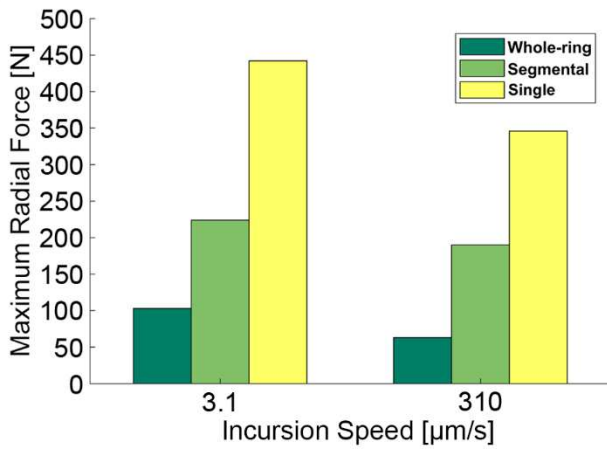


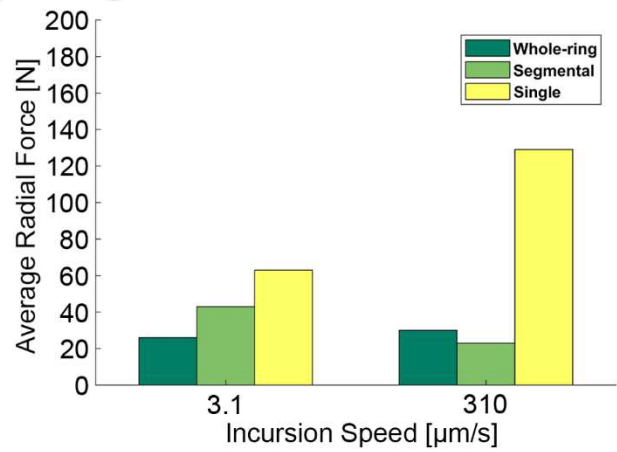
Figure 9 Force and temperature results at low incursion speed (0-2700 rub length) with a) whole-ring fin, b) segmental fin and c) single discrete fin (replotted from Figure 8)

In order to further analyse the trends seen in the tests, the maximum and average, forces and temperatures were extracted from the results and compared (Figure 10). As shown in the figure, the previously discussed trends with respect to incursion speed and fin type are clearly evident. A broadly consistent trend with respect to force is shown, with the discrete fin having the higher contact forces, followed by the segmented test, and finally the whole ring (Figures 10a-d). This trend is particularly apparent at the lower incursion speed with respect to both radial and tangential forces. At the higher incursion speed the results for the whole ring and segment overlap to a degree, whilst the discrete fin still clearly has the highest forces. Finally, it is also interesting to note that there is no clear trend of increasing force with incursion speed, and indeed in some cases forces are reduced. Given the upper incursion speed is 100 times higher than the lower rate, meaning a significantly larger amount of material is removed per revolution, no substantial change in force is indicative of a movement to a more efficient material removal mechanism, and this will be investigated further by investigating the cut surface of the abrasible. Comparing temperatures, a clear trend is also apparent with the whole ring and segment having higher maximum and average temperatures than the discrete fin (Figure 10e-f). At both the upper and lower peak incursion rates, the highest temperatures are consistently recorded for the segmented fin. Finally, a trend is also apparent of reducing temperature with incursion rate for both the segmented and whole ring tests.

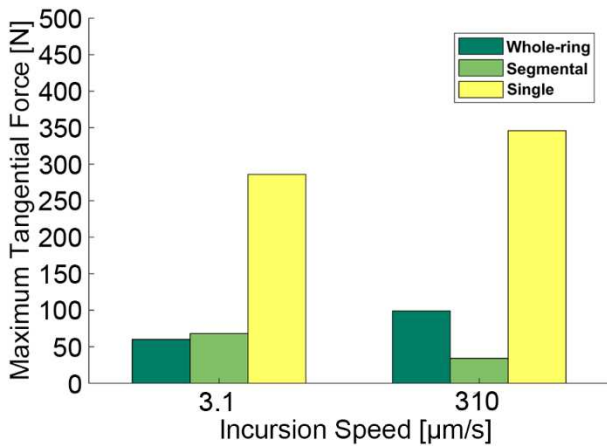
a) Maximum radial force



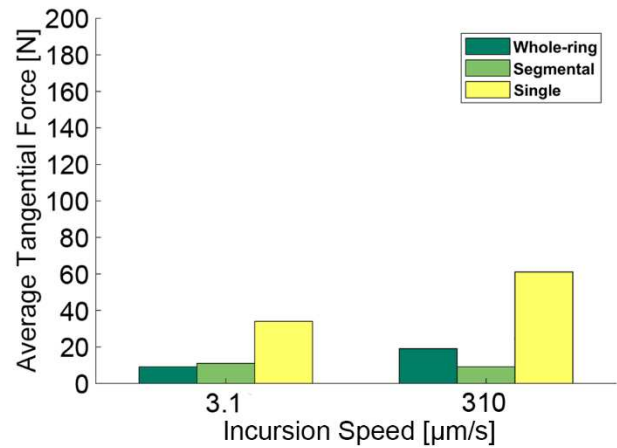
b) Average radial force



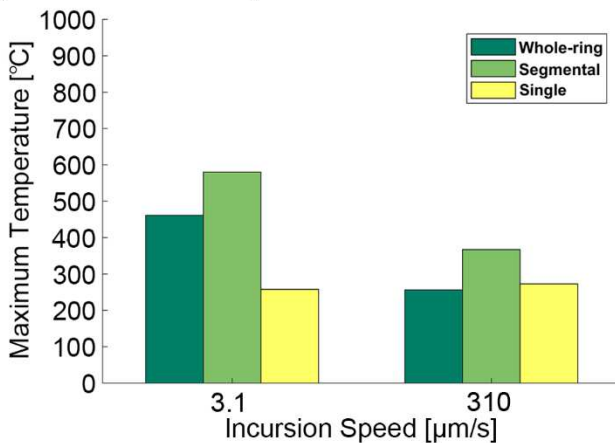
c) Maximum tangential force



d) Average tangential force



e) Maximum temperature



f) Average temperature

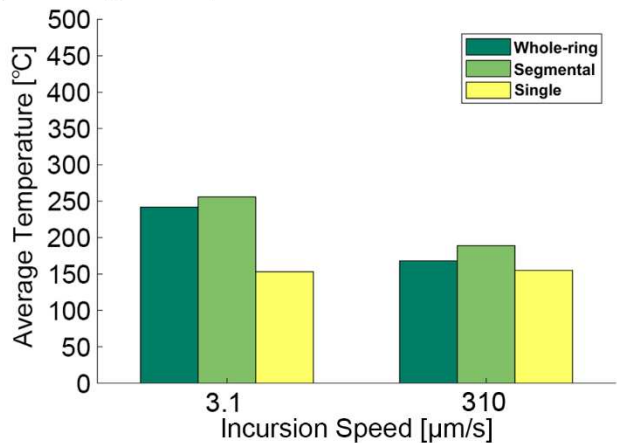


Figure 10 Bar charts of maximum and average forces for whole-ring segmental and single discrete fin tests, a) maximum radial force, b) maximum tangential force and c) maximum temperature

3.3 Wear groove surface microscope images

Figure 11 shows images taken from the centre of each of the worn grooves on the abradable samples tested. As shown in the figure, distinct differences in surface condition with respect to both incursion rate and fin type are present. At the low incursion speed condition (Figure 11a-c) a surface containing irregular shiny areas is present, interrupted by fractured areas where material has been removed. Chips of loose material are also evident on the surface in some instances (Figure 11a). Comparing back to previous studies [2], this type of surface morphology has been linked to a compressive mechanism, where at the exhaustion of ductility, material ruptures and is removed from the contact. This mechanism was proposed to be cyclic, building

sequentially over multiple passes, with looser material also removed with each blade interaction. Looking back to the Figure 11, it is interesting to note that significantly more extruded material is present for the segmented fin and whole ring (Figures 11a and 11b respectively), when compared to for a discrete fin (Figure 11c). It also appears that the most material affected in this way is for the segmented fin, and this may indeed be linked in some way to the higher temperatures recorded for this case. Moving to the higher incursion speed (Figure 11d-f) all of the wear scars display a similar morphology, with a well-cut surface present. Whilst it is difficult to tell if the material removal mechanism is identical in each of these cases, with this unlikely to be the case due to the different lengths of the fin segments tested, and an increased propensity for impact as opposed to rubbing with the discrete fin due to its short contact duration, the final outcome is similar. Previous studies [2] also highlight material as extruded out of the contact, with the results here consistent with good abrasible release.

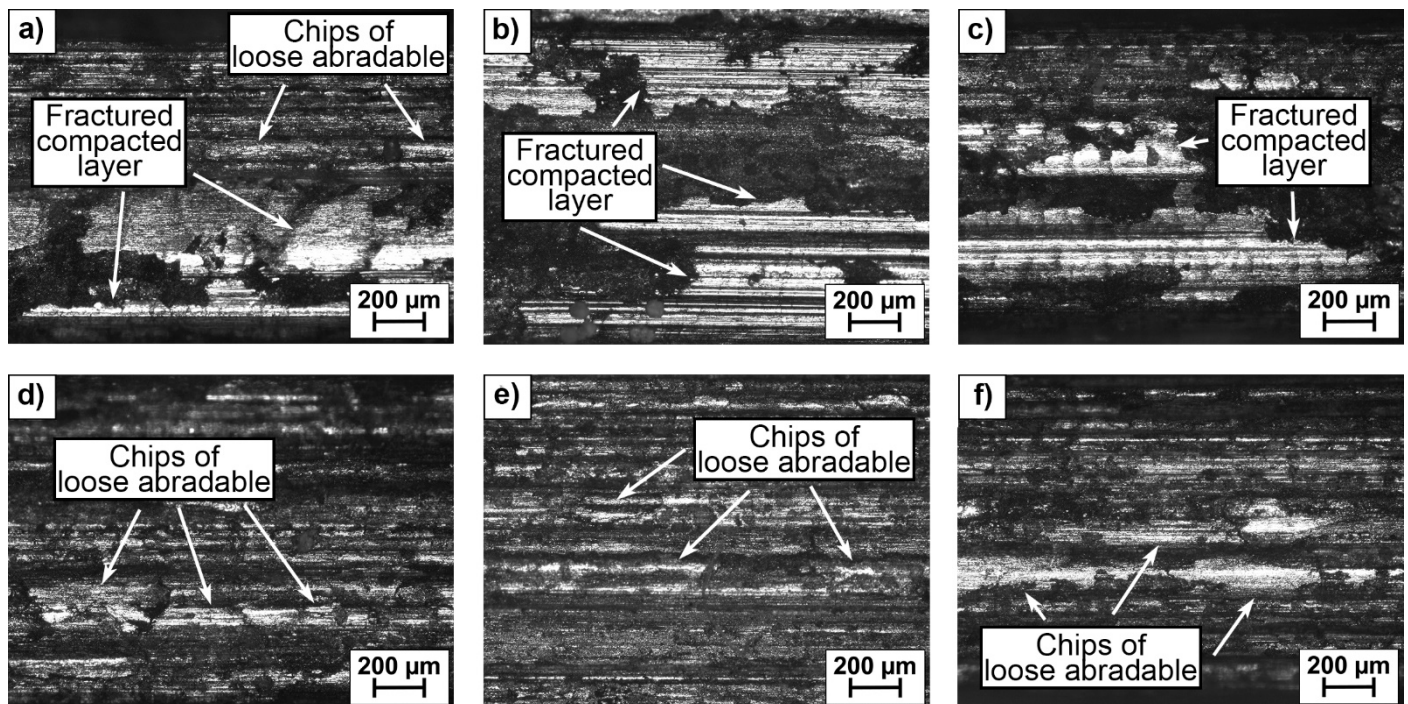


Figure 11 Wear groove surface microscope copies of the tests with three types of St.St.304 fin, a) whole ring, 0.02μm/pass, b) segmental, 0.02μm/pass, c) single discrete, 0.02μm/pass, d) whole ring, 2μm/pass, e) segmental, 2μm/pass, and f) single discrete

3.4 SEM analysis of the rub debris

Using the particles collected via the SEM stubs, further insight could be gained into the material removal mechanism. As shown in Figure 12, generally the debris collected during the test can be classified into one of two types. The first of these two types is flake shaped debris (size 0.1~0.3mm) in the form of chips. This type of wear debris is present in all of the tests, with the exception of that for the discrete fin at the higher incursion rate. It is also apparent that this flake shaped debris is particularly apparent at the low incursion condition (Figures 12a-c), and appears to consist of the material removed via the fracture of the extruded layer on the abrasible surface detailed previously (Figures 11a-c). The second type of debris observed was smaller and particulate in nature (size 1μm to 100μm). This type of debris was to a degree present in all tests, but it is interesting to note that it was the sole form of debris at the higher incursion rate for the discrete fin (Figure 12f). Looking further into the relationship between fin type, incursion speed and debris morphology, the results for the segmented fin stand out. At both the high (Figure 12e) and low (Figure 12b) incursion

speeds, particulate debris is minimal, with larger flakes of material dominating. Going back to the results detailed for wear scar morphology and indeed temperature for this fin type, it would appear that the occurrence of larger flakes of debris links well to the previous discussion around increased extrusion and temperature. Finally, considering all of the different fin types present, it is seen that there is an increased propensity for particulate debris at the higher incursion speed, with this presumably linked to an enhanced cutting mechanism and material removal from the surface.

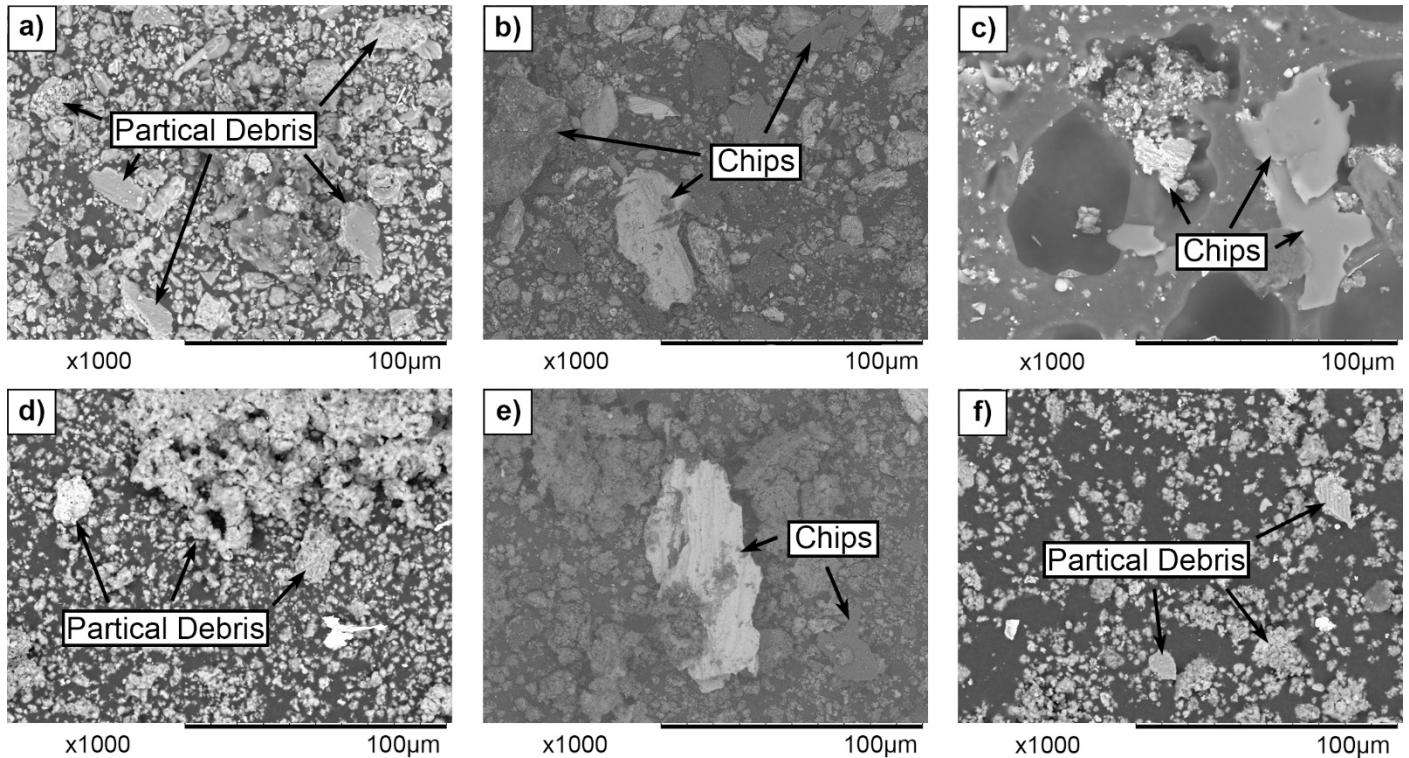


Figure 12 Debris SEM images of all tests with three types of St.St.304 fin, a) whole ring, 0.02µm/pass, b) segmental, 0.02µm/pass, c) single discrete, 0.02µm/pass, d) whole ring, 2µm/pass, e) segmental, 2µm/pass and f) single discrete, 2µm/pass

4 Discussion

From the results detailed in the previous section, it can be observed that the dominant factor which affects the abradable material removal mechanism is incursion speed. For all of the different fin types investigated, at a low incursion speed, material is removed via a process of compaction and fracture. This process is cyclic in nature, and is evident in both the nature of the forces and temperatures recorded, as well as the morphology of the wear scar and debris generated. One variation with fin type that is evident from these results is how well debris is able to exit the contact, where increasing levels of smeared material are evident when a longer fin contact occurs. Conversely, with the short fin, smaller fractured particles occur. At the higher incursion speeds, good removal of the abradable material is evident, with this clear from all measures. However, it is also noticeable once again that for the longer fins, and in particular for the segmented test sample, that larger, extruded chips of material are also formed. Comparing back to previous results [2,10*], the influence of incursion speed is well documented, and the expected transition from compression / release through to displacement of material occurs as this parameter increases. However, it is interesting to note the influence of fin length on these two mechanisms, and this requires further consideration.

As highlighted by Figures 10e & 10f, a clear trend in temperature is observed with respect to fin type, with the segmented fin recording the highest peak and average temperatures at the surface for each incursion

condition. Given the different fin shapes, the heat-generation and dissipation methods are also different in each case. Going back to the abradable material removal mechanism previously detailed for fins [2], this suggests that heat in the contact is primarily generated in one of two ways: either by frictional heating in the fin-abradable contact, or through the process of cutting. This heat is then dissipated via either thermal conduction through the fin or abradable, or the release of hot debris from the contact, with convection and radiation to the surrounding environment assumed negligible in comparison with the two aforementioned mechanisms. This relationship can be expressed as follows:

$$Q_c = Q_{tca} + Q_{tcf} + Q_s \quad \text{Equation 3}$$

where Q_c is the heat input due to the material removal process inclusive of frictional heating, Q_{tca} and Q_{tcf} are the conductive heat transfer to the abradable and fin respectively, and Q_s the heat dissipated by sparking. In this equation, the heat input Q_c , mainly driven by the cutting energy, is generated during the chip formation process, and can be considered as a product of the cutting speed and un-deformed chip thickness [16]:

$$Q_c = F(v_c, \delta) \quad \text{Equation 4}$$

where v_c is the cutting speed, and δ the un-deformed chip thickness. As detailed by Balogun [17] and Aramcharoen [18], in a typical chip formation process there are three different types of interaction: rubbing, ploughing and shearing. They then go on to detail that the mechanism is determined by the ratio of the un-deformed chip thickness to the cutting-edge radius (R_h). If this ratio is less than one, the trend is towards rubbing; equal to one ploughing occurs, and as the ratio exceeds one, shearing becomes dominant. In the case of the fins used in this study, the discrete fin and segment have a corner radius of 2mm, which is much larger than the un-deformed chip thickness in each case (for example this is 0.02-2 μ m in the case of the discrete fin). In the case of the whole ring, continuous contact occurs. Therefore, after considering the different contacts present, rubbing is clearly the dominant material removal mechanism, with this being in line with observations in this study as well as those previously [2]. Given the fact rubbing is identified as the dominant material removal mechanism, the heat removal via the ejection of hot material in the form of sparks (Q_s) is assumed negligible, as the importance of this term directly relates to the amount of cutting taking place.

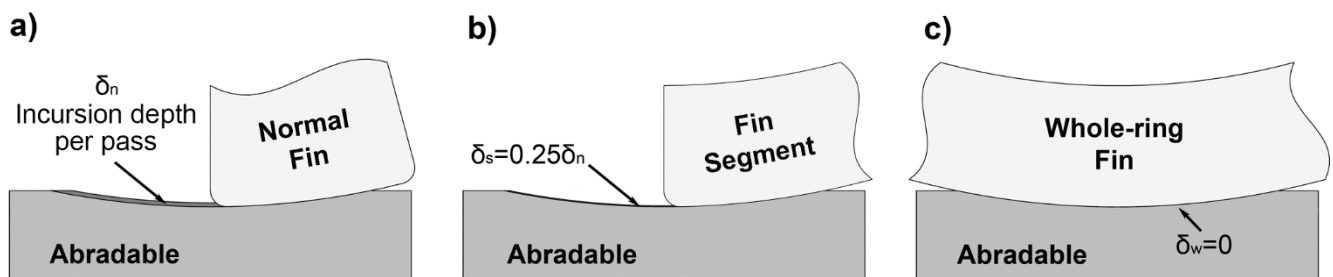


Figure 13 Schematic diagrams for a single pass of a) single discrete fin, b) fin segment and c) whole-ring fin

Figure 13 shows a schematic diagram for a single pass for the different fin shapes. Illustrated on the figure is the un-deformed chip thickness (incursion depth per pass of the fin) for the single discrete fin, δ_n , and the corresponding values for the fin segment and whole ring, expressed relative to that of the discrete fin. In the case of the test with the fin segment, in a single revolution two segments interact with the abradable (diametrically opposed, spaced at 90 degrees), meaning the maximum period of non-contact is a quarter

revolution, and the un-deformed chip thickness is a quarter that of the discrete fin. Finally, for the whole ring, as previously noted, a continuous contact occurs, and the un-deformed chip thickness is zero. According to the experimental results published by Balogun [16, 17, 19], the specific cutting energy has an exponential relationship with the ratio of corner radius to un-deformed chip thickness, and increases rapidly as this ratio becomes significantly less than 1, and the transition to pure rubbing occurs.

Going back to the heat passing to the abradable and fin via conduction, as detailed by Kato and Fuji [20], the heat flow in a machining contact between tool and workpiece can be related to the heat partition coefficient. The heat partition coefficient is a product of the specific heat capacity, density and thermal conductivity of the materials in the contact, and is expressed as follows:

$$\frac{Q_{tcf}}{Q_{tca}} = \frac{(c_p \rho \lambda)_{fin}}{(c_p \rho \lambda)_{abradable}} \quad \text{Equation 5}$$

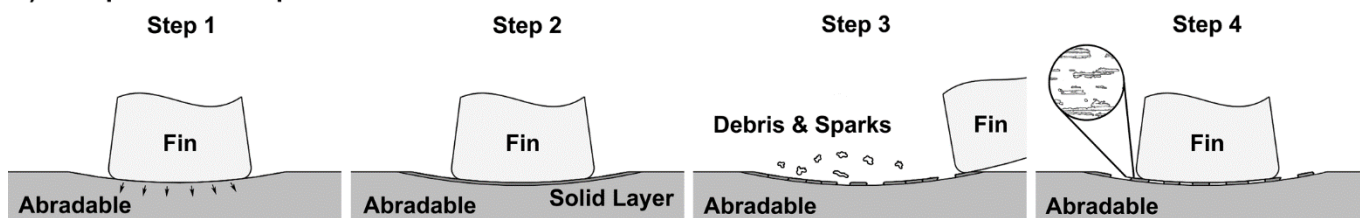
Q_{tcf} and Q_{tca} are the conductive heat transfer to the abradable and fin respectively, and c_p the specific heat capacity, ρ density, and λ thermal conductivity of both the abradable and fin materials. Table 2 shows the aforementioned properties for the fin and abradable used in this study, along with the calculated heat partition coefficient. As shown in the table, approximately 40% more heat flows into the fin, as opposed to the abradable, making this the preferential heat transfer path from the contact when fin and abradable touch.

Table 2 Thermal properties of the test samples and heat partition coefficient

Contact Body	Material	Specific Heat Capacity [J(g K) ⁻¹]	Thermal Conductivity [W(m K) ⁻¹]	Density [gcm ⁻³]	Heat Partition Coefficient (Q_{tcf} / Q_{tca})
Fin	Stainless Steel	0.502	16.2	7.85	1.41
Abradable	M601	1.174	21.8	1.77	

The heat partition coefficient along with the aforementioned discussion with respect to heat generation in the incursion event, can be used to explain the observed results at each condition tested. Considering first the discrete fin, this is the most efficient material removal mechanism meaning the least heat is generated. However, as the contact duration is short, limited time is available for heat to conduct from the contact zone to the fin. Overall, this leads to high, but not the highest temperatures. Moving to the segment, significant heat is now generated as a consequence of the rubbing mechanism present. The heat generated is able to flow to the fin for half of the time during a revolution (as two fin segments are used diametrically opposed, spaced by 90 degrees), meaning relatively effective heat transfer occurs. Overall, this results in higher temperatures for the segment when compared to the discrete fin, although an extreme event is avoided. Finally, for the whole ring the least efficient material removal mechanism occurs, meaning in order to remove the abradable material the most heat will be generated. However, as this process is continual, the heat generated is more evenly distributed around the circumference of the disc, with the fin providing a constant heat sink for the contact. As a consequence, temperatures generated in the abradable are slightly lower than for the segment, but higher than for the discrete fin due to the inefficiencies in material removal mechanism outlined. The thermal model detailed also explains the differences in temperature (Figures 10e and 10f) seen between incursion rates for the different fins, where lower temperatures occur at the higher incursion rate, corresponding with a slightly more efficient material removal mechanism.

a) Compact-fracture process



b) Extrusion process

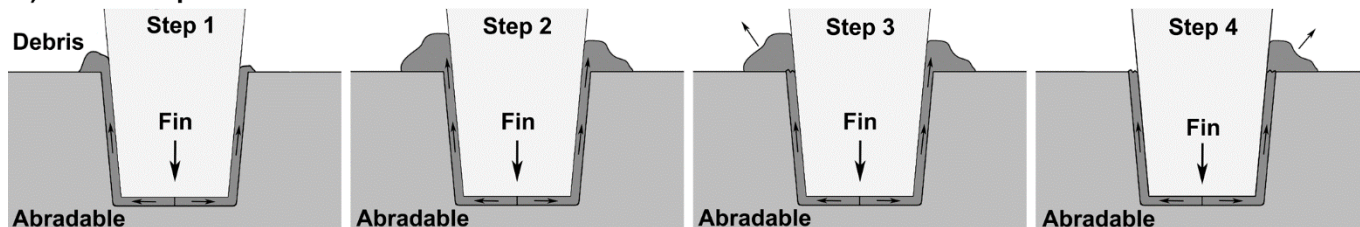


Figure 14 Two abrasible material removal mechanisms, a) compact-fracture process and b) extrusion process [2]

As detailed in the previous discussion, the geometry of the fin sample influences the material removal mechanism, leading to changes in the temperatures generated. This in turn leads to differences with respect to both forces measured, wear scar morphology, and debris as detailed in Section 3. In a previous study [2] the material removal mechanism for a discrete fin in contact with an abrasible has been well documented at both high and low incursion conditions. Figure 14 shows the mechanism determined in the study, where at low incursion rates cyclic compaction and fracture takes place with limited extrusion from the side of the contact (Figure 14a), and at high rates extrusion from the contact occurs (Figure 14b). In the present study, this improving material removal mechanism from low to high incursion rate results in similar forces for the two conditions, even though significantly more material is removed per pass at the higher rate, and a progression to a fractured wear scar and associated debris.

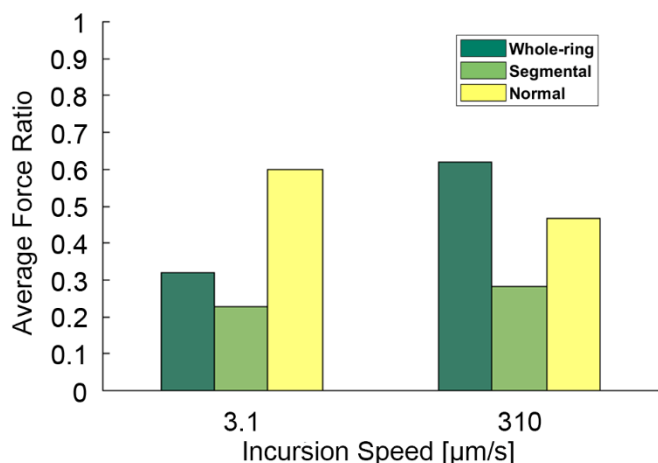


Figure 15 Average Force Ratio

As discussed, the material removal mechanism changes for both the segment and whole ring test fins, and increased rubbing takes place leading to higher surface temperatures. Comparing the force ratios for the different incursions (Figure 15), a difference in mechanism is also apparent. This measure is the most appropriate to consider any mechanism change, as the force ratio normalises the force results with respect to the varying chip thickness present. As shown in the figure, in particular for the low incursion rate tests for the segment and whole ring, the force ratio is lower, indicating lower friction in the contact, with previous studies suggesting this is due to material reaching a semi-molten state [12]. This is further evidenced by the

observations seen in the wear scar and debris generated, where for these two samples increased smearing and chips of material are observed respectively. At the higher incursion rate the trend is less clear, with the force ratio indicating some cutting alongside rubbing takes place for the whole ring in particular and the segment to a degree, but reduced in volume when compared to the discrete fin. This conclusion is in line with the previously discussed temperature results, where greater smearing would be expected for segment test at this incursion rate, given the higher thermal conditions measured. Further evidence of this mechanism difference is also found in the wear scars and debris collected, where for the discrete fin less smearing is found in the wear scar and particulate debris is generated, when compared to the segment and whole ring, where some smearing in the rub track along with chip like debris is still observed. However, it should be noted that the difference detailed in force and temperature results for the segment and whole ring is less evident in the wear scar and debris images. Overall though, when compared to the discrete fin tests, these results do show that at both incursion rates, increasing the length of the contact does influence the material removal mechanism. Whilst changes were not significant in this case, this depends on the relative thermal properties of both the abradable and fin sample, and in some cases may lead to a significant change in material removal mechanism (i.e. from cutting to rubbing) where interface temperatures change. For example, in studies performed by Bayata on iron-nickel steel (NCF3015) and nickel based superalloy (IN751) samples, changes in the thermal/mechanical properties of the components in contact resulted in a transition from an abrasive wear mechanism to one of melt wear [21]. This behaviour was similarly observed by Hao when investigating IN625 superalloys [22]. Such changes in behaviour is not only just observed during the wear testing of metal alloys. For example, a transition in wear mechanism also occurred for thermally sprayed coatings (TiB2-50Ni) in research conducted by Wang et. al. [23] as thermal properties were varied. As such, contact conditions should be carefully considered when testing fin samples, and caution applied when interpreting results.

5 Conclusions

This study determined the influences of test specimen when investigating the contact between abradable materials and fins in aero-engines, it was confirmed that:

- The material removal mechanism was influenced at both the high and low incursion conditions by the length of the fin contact, with this due to both the influence of increasing contact length on chip thickness, as well as on the thermal behaviour of the system.
- Changes in material removal mechanism were evident at both the high and low incursion condition, but more pronounced at the lower rate, where a greater propensity for rubbing already existed.
- A discrete fin was observed to trigger a more efficient material removal mechanism at both incursion conditions, with the fin segment and whole ring leading to increased temperatures and material smearing.
- The fin segment was observed to promote smearing the most, as it was long enough to trigger significant rubbing, but compromised in terms of heat removal when compared to the continuous contact of the whole ring.
- The outlined changes in material removal mechanism led to differences in both the wear scar morphology and debris generated, and when using such testing to investigate aspects of aero-engine behaviour, a clear understanding and matching of contact conditions is required, and if for example thermal wear is being investigated, a whole ring contact is preferable.
- This work also highlights the role of the fin material in removing heat from the contact, with the opportunity to minimise thermal damage in the abradable – fin system via careful consideration of the thermal properties of the fin.

References

1. Zhang B and Marshall M. Investigating the application of a honeycomb abradable lining in the turbine stage of an aero-engine. 2018. *Tribology International* 2018; 125: 66-74. DOI: 10.1016/j.triboint.2018.04.013
2. Zhang B and Marshall M. Investigating material removal mechanism of Al-Si base abradable coating in labyrinth seal system. *Wear* 2019; 426–427 (A): 239-249. DOI: 10.1016/j.wear.2019.01.034
3. Rolls-Royce plc., *The jet engine*. 5th ed. 1996, ISBN: 0902121235
4. Delebarre C, Wagne V, Paris JY, Dessein G, Denape J and Gurt-Santanach J. An experimental study of the high speed interaction between a labyrinth seal and an abradable coating in a turbo-engine application. *Wear* 2014; 316: 109-118. DOI: 10.1016/j.wear.2014.04.023
5. Delebarre C, Wagne V, Paris JY, Dessein G, Denape J and Gurt-Santanach J. The wear mechanisms occurring in a labyrinth seal-abradable contact depending on the incursion depth parameter. *Mechanics & Industry* 2016; 17. DOI: 10.1051/meca/2015118
6. Delebarre C, Wagne V, Paris JY, Dessein G, Denape J and Gurt-Santanach J. Tribological characterization of a labyrinth-abradable interaction in a turbo engine application, *Wear* 2017; 370-371: 29-38. DOI: 10.1016/j.wear.2016.11.007
7. Pychynski T, Höfler C and Bauer H. Experimental study on the friction contact between a labyrinth seal fin and a honeycomb Stator. *Journal of Engineering for Gas Turbines and Power* 2016; 138: 062501-1-062501-9. DOI: 10.1115/1.4031791
8. Munz O, Pychynski T, Schwitzke C and Bauer H. Continued experimental study on the friction contact between a labyrinth seal fin and a honeycomb stator: slanted position. *Aerospace* 2018; 5(3): 82-1-82-16. DOI: 10.3390/aerospace5030082
9. Thévenota M, Wagnera V, Parisa J-Y, Desseina G, Denapea J, Harzallaha M, Brunetb A, Chantraic T. Thermomechanical phenomena and wear flow mechanisms during high speed contact of abradable materials. *Wear* 2019; 426-427: 1102-1109. DOI: 10.1016/j.wear.2019.01.094
10. Lu B, Ma X, Wu C, Xuan H, Hong W. The wear of seal fins during high-speed rub between labyrinth seal fins and honeycomb stators at different incursion rates. *Materials (Basel)* 2021;14(4): 979. DOI: 10.3390/ma14040979.
11. Fois N, Stringer J and Marshall M. Adhesive transfer in aero-engine abradable linings contact. *Wear* 2013; 304 (1-2): 202-210. DOI: 10.1016/j.wear.2013.04.033
12. Fois N, Watson M, Stringer J and Marshall M. An investigation of the relationship between wear and contact force for abradable materials. *Proceedings of the Institution of Mechanical Engineers, Part J: Journal of Engineering Tribology* 2014; 229(2): 136-150. DOI: 10.1177/1350650114545139
13. Watson M, Fois N and Marshall M. Effects of blade surface treatments in tip -shroud abradable contacts. *Wear* 2015; 338-339: 268-281. DOI: 10.1016/j.wear.2015.06.018

14. Liu Y D, Zhang J P, Pei Z L, Liu J H, Li W H, Gong J, Sun C. Investigation on high-speed rubbing behavior between abrasive coatings and Al/hBN abradable seal coatings. *Wear* 2020; 456-457: 203389. DOI: 10.1016/j.wear.2020.203389
15. Fois N, Watson M and Marshall M. The influence of material properties on the wear of abradable materials. *Proceedings of the Institution of Mechanical Engineers, Part J: Journal of Engineering Tribology* 2016; DOI: 10.1177/1350650116649528
16. Balogun VA, Gu H and Mativenga PT. Improving the integrity of specific cutting energy coefficients for energy demand modelling. *Proceedings of the Institution of Mechanical Engineers, Part B: Journal of Engineering Manufacture* 2014; 229(12). DOI: 10.1177/0954405414546145
17. Balogun VA, Edem IF, Adekunle AA and Mativenga PT. Specific energy based evaluation of machining efficiency. *Journal of Cleaner Production* 2016; 116: 187-197. DOI: 10.1016/j.jclepro.2015.12.106
18. Aramcharoen A and Mativenga PT. Size effect and tool geometry in micromilling of tool steel. *Precision Engineering* 2009; 33(4): 402-407. DOI: 10.1016/j.precisioneng.2008.11.002
19. Balogun VA and Mativenga PT. Impact of un-deformed chip thickness on specific energy in mechanical machining processes. *Journal of Cleaner Production* 2014; 69: 260-268. DOI: 10.1016/j.jclepro.2014.01.036
20. Kato T and Fujii H, Energy Partition in Conventional Surface Grinding. *Journal of Manufacturing Science and Engineering* 1999; 121: 393-398.
21. Bayata F and Alpas A. The high temperature wear mechanisms of iron-nickel steel (NCF 3015) and nickel based superalloy (inconel 751) engine valves. *Wear* 2021; p. 203943. DOI: 10.1016/j.wear.2021.203943
22. Hao J, Hu F, Le X, Liu H, Yang H and Han J. Microstructure and high-temperature wear behaviour of Inconel 625 multi-layer cladding prepared on H13 mould steel by a hybrid additive manufacturing method. *Journal of Materials Processing Technology* 2021; 291: 117036. DOI: 10.1016/j.jmatprotec.2020.117036
23. Wang Y, Zhang W, Chen D, Liu X, Hu W, Liu L, Yan J and Xiong X. High temperature friction and wear performance of TiB₂-50Ni composite coating sprayed by HVOF technique. *Surface and Coatings Technology* 2021; 407:126766. DOI: 10.1016/j.surfcoat.2020.126766